

Transport properties of Keplerian flows in extended local domains with no imposed field

Farrukh Nauman^{1*}, Martin E. Pessah^{1†}

¹*Niels Bohr International Academy, The Niels Bohr Institute, Blegdamsvej 17, DK-2100, Copenhagen Ø, Denmark.*

6 February 2022

ABSTRACT

We compare transport statistics of elongated incompressible shearing boxes for different Reynolds and magnetic Prandtl numbers, Re and Pm , and aspect ratios, L_z/L_x . We find that at fixed aspect ratio $L_z/L_x = 4$ and $Re = 10,000$, the turbulent stresses for $Pm \lesssim 1$ do not show considerable variation and follow a power law $\sim Pm^{3/2}$ for $Pm > 1$. This is qualitatively consistent with previous results based on net imposed flux and small box $L_z/L_x \sim 1$ simulations but the power law exponent is different. The saturated level of stresses, the ratio of Maxwell stress to the magnetic energy and Reynolds to Maxwell stress ratio are roughly invariant as L_z/L_x is increased. For cases where the boxes are elongated in both the azimuth and vertical direction, the transport coefficient $\alpha \in [0.1, 1.0]$ that is 10 – 100 times larger than the case with $L_y/L_x = 2$ and large L_z/L_x . Overall, our results suggest that the saturated state of turbulence is sensitive to both dissipation coefficients and aspect ratio (both L_z/L_x , L_y/L_x) motivating further work on this problem.

Key words: accretion, accretion disks — magnetohydrodynamic turbulence

1 INTRODUCTION

Accretion flows exist in a variety of astrophysical systems. The accreting fluid would have a much longer lifetime if molecular viscosity was the sole source of angular momentum transport. For this reason, a number of possible alternative transport mechanisms have been investigated in recent years ranging from purely hydrodynamic sources to magnetohydrodynamic sources. Evaluating each of these mechanisms in detail and understanding their observational implications is a subject of ongoing research (Balbus & Hawley 1998; Fromang & Lesur 2017).

Magnetized Keplerian flows are linearly unstable to the magnetorotational instability (MRI) if a weak external magnetic field is present (Velikhov 1959; Chandrasekhar 1960; Balbus & Hawley 1991). The MRI has been studied extensively in local shearing box simulations (Hawley et al. 1995; Brandenburg et al. 1995; Fromang et al. 2007), global disk simulations (Flock et al. 2012; Parkin & Bicknell 2013; Suzuki & Inutsuka 2014; Zhu & Stone 2018) and Taylor-Couette flow simulations (Wei et al. 2016; Guseva et al. 2017b,a). Despite more than two decades of numerical work on the problem, the issue of convergence is still unresolved with work focusing on imposed field, the presence of dissipation coefficients, density stratification due to gravity (Fromang & Papaloizou 2007; Davis et al. 2010; Hawley et al. 2011; Bodo et al. 2014; Meheut et al. 2015; Ryan et al. 2017).

If the external flux is removed in a magnetized Keplerian flow, then the fluid is no longer linearly unstable to MRI but is yet observed to reach a nonlinear steady state with significant transport (Hawley et al. 1996; Fromang et al. 2007; Lesur & Ogilvie 2008; Guseva et al. 2017a). In the literature, this case is sometimes referred to as the ‘dynamo’ case but we do not use such terminology here because in a broad sense, fluids linearly unstable to MRI are also an example of a dynamo since they lead to the generation and sustenance of magnetic fields (Gressel & Pessah 2015). The ‘zero flux’ case has been a particular focus of numerical studies trying to seek convergence since it was realized that the increase in resolution leads to a decrease in transport (Pessah et al. 2007; Fromang & Papaloizou 2007).

The role of Reynolds number as an important parameter in shear flows is well known since the original work of Reynolds in 1883. The realization that the aspect ratio might also play an important role in determining the nonlinear state of a fluid came much later (Cross & Hohenberg 1993; Philip & Manneville 2011). Moreover, recent numerical and experimental work on shear flows suggests that small domains might suffer from finite size effects at transition (Lemoult et al. 2016) and that the transition to turbulence in shear flows perhaps belongs to the directed percolation universality class (Pomeau 1986).

Until recently, Keplerian flows without a net imposed

* E-mail: nauman@nbi.ku.dk

† E-mail: mpessah@nbi.dk

flux were thought to be stable for magnetic Prandtl number at and below unity (Fromang et al. 2007). However, Nauman & Pessah (2016) (Paper I) showed that if a large aspect ratio ($L_z/L_x \geq 4$) is used, then flows can still reach a nonlinear steady state with magnetic Prandtl number below unity. The transport properties of such elongated boxes was not addressed in that paper. The focus of the current paper is to explore the dependence of turbulent transport on box size, Reynolds number and magnetic Prandtl number.

That the aspect ratio plays an important role has gained further support from recent work by Shi et al. (2016) and Walker & Boldyrev (2017) with the observation that larger aspect ratios allow for local non-zero toroidal magnetic flux. Using ideal compressible MHD simulations, Shi et al. (2016) showed not only that the turbulent stresses in boxes with $L_z/L_x > 2.5$ converged with respect to increasing resolution but also that the saturated level of stresses was insensitive to further increase in the aspect ratio. The bulk of their work was using ideal MHD and while Shi et al. (2016) did some numerical simulations with explicit dissipation coefficients, a more comprehensive survey of the effects of aspect ratio in the presence of dissipation has yet to be carried out.

The goal of this paper is to study the transport properties as a function of aspect ratio and dissipation coefficients. The organization of this paper is as follows: Section 2 describes the numerical setup. Section 3 reports on transport properties of large aspect ratio systems as a function of Re , Pm and L_z . We then present resolution tests in section 4. In section 5, we describe the results from simulations where the domain is extended in both ‘y’ and ‘z’. We conclude in section 6.

2 NUMERICAL SETUP

Using the publicly available pseudospectral code SNOOPY¹ (Lesur & Longaretti 2007), we solved the incompressible MHD simulations in the shearing box framework:

$$\frac{\partial \mathbf{v}}{\partial t} + \mathbf{V}_{sh} \frac{\partial \mathbf{v}}{\partial y} + \nabla \cdot \mathbf{T} = 2\Omega v_y \mathbf{e}_x - (2 - q)\Omega v_x \mathbf{e}_y + \nu \nabla^2 \mathbf{v}, \quad (1)$$

$$\frac{\partial \mathbf{b}}{\partial t} = \nabla \times (\mathbf{V}_{sh} \times \mathbf{b}) + \nabla \times (\mathbf{v} \times \mathbf{b}) + \eta \nabla^2 \mathbf{b}, \quad (2)$$

$$\nabla \cdot \mathbf{v} = 0, \quad (3)$$

$$\nabla \cdot \mathbf{b} = 0, \quad (4)$$

where \mathbf{v} and \mathbf{b} are the velocity and magnetic field respectively. Here \mathbf{T} is a stress tensor given by

$$\mathbf{T} = (p + b^2/2)\mathbf{I} + \mathbf{v}\mathbf{v} - \mathbf{b}\mathbf{b}, \quad (5)$$

where \mathbf{I} is the identity matrix and p is thermal pressure.

We impose no external magnetic flux. The magnetic field is initialized with a sinusoidal profile: $\mathbf{B}_{ini} = B_0 \sin(k_x x) \mathbf{e}_z$. The background velocity profile is given by $\mathbf{V}_{sh} = -Sx \mathbf{e}_y$, where $S = q\Omega = 1$ ($q = -d \ln \Omega / d \ln r = 3/2$ for Keplerian shear) is the shear parameter and Ω is the angular frequency. Since this state is linearly stable, we have to apply large amplitude perturbations to trigger nontrivial dynamics. The perturbations are of magnitude LS applied

to large scale velocity modes. The time unit in our simulations is the shear time, $1/S$ ($\sim 1/10$ orbits where 1 orbit = $2\pi/\Omega$). The magnetic field has the units of the Alfvén speed and $\mu_0 = 1, \rho_0 = 1$. The Reynolds and magnetic Reynolds numbers are $Re = SL_x^2/\nu$ and $Rm = SL_x^2/\eta$, respectively (with $L_x = 1$ and $Pm = Rm/Re$). We point out that the definition of Re and Rm we use is different from some of the previous works we refer to: compressible studies typically take the pressure scale height, H , as the length scale instead of L_x while L_z has been used by Lesur & Longaretti (2007) for incompressible studies.

3 LARGE ASPECT RATIO: $L_z/L_x \geq 4$

We describe the different transport properties in this section. Note that, unless otherwise indicated, all quantities are volume averaged over the entire domain and time averaged over $500 - 10000 S^{-1}$ (or roughly $50 - 1000$ orbits except for $L_z = 32$ which was only averaged over $500 - 1000 S^{-1}$). In the following, we compare our results with the only other study that focused on aspect ratio dependence of transport coefficients, Shi et al. (2016). It is important to mention two key differences in their simulations and ours: Shi et al. (2016) use ideal MHD for most of their work and solve compressible MHD equations. We, on the other hand, have run incompressible simulations with explicit dissipation coefficients. Moreover, we focus our attention to studying the effect of varying aspect ratios and dissipation coefficient at the same resolution while Shi et al. (2016) focused on resolution studies for different aspect ratios and had a small fraction of runs including explicit dissipation. A resolution study is presented in section 4 that does not show drastic differences between the resolution adapted for most of this work ($64/L_x$) and higher resolutions ($128/L_x, 256/L_x$). We also point out that the runs $L_z/L_x = 16, 32$ are new to this paper and were not part of the study in Paper I.

3.1 Fixed $Re = 10,000, Pm = 1$, variable L_z

Shi et al. (2016) demonstrated using compressible ideal MHD simulations that the stresses converge with respect to resolution for $L_z/L_x \geq 2.5$ and that this saturation level was nearly independent of the aspect ratio beyond $L_z/L_x = 2.5$. In our incompressible simulations, we could not find any sustained turbulence for $L_z/L_x < 4$ at $Pm = 1$ so we are unable to confirm if $L_z/L_x = 2.5$ defines a threshold for convergence. In fig. 1, we plot the volume averaged stress, $\alpha = \langle v_x v_y - b_x b_y \rangle / S^2 L_x^2$ as a function of L_z , which seems to be slightly sensitive to the aspect ratio but does not show great variation going from $L_z/L_x = 4$ to 32 . In the middle panel, we plot the Maxwell to Reynolds stress ratio, which seems to converge between $5 - 6$. Both this and the α convergence are consistent with Shi et al. (2016) results (see their figures 6 and 7). The bottom panel shows that $\alpha_{mag} = \langle -b_x b_y / b^2 \rangle$ remains approximately invariant $0.40 - 0.43$ as the aspect ratio is increased. This differs from the behavior reported in fig. 8 of Shi et al. (2016), where they found that the α_{mag} decreased with increasing aspect ratio as $(L_z/L_x)^{-1/2}$.

¹ <http://ipag.osug.fr/~lesurg/snoopy.html>

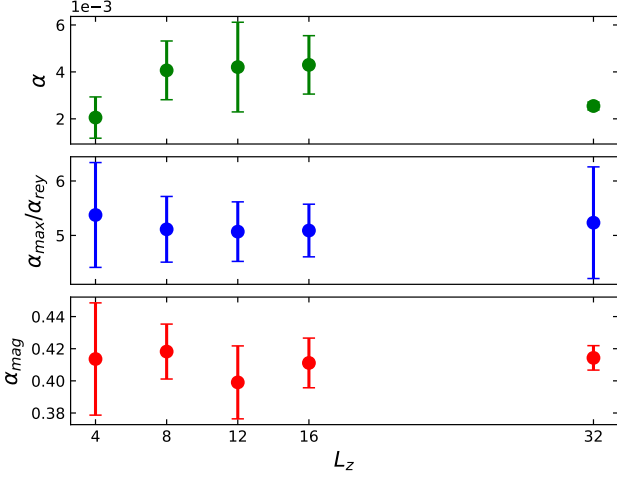


Figure 1. The volume averaged stress, $\alpha = \langle v_x v_y - b_x b_y \rangle / S^2 L_x^2$ that was further averaged over time from $t = 500 - 10000 \text{ S}^{-1}$ (except $L_z = 32$ that was averaged in the range $250 - 1000 \text{ S}^{-1}$) at $Re = 10,000, Pm = 1$ as a function of different L_z . *Top:* The stresses at $L_z/L_x \geq 8$ are all higher than the $L_z/L_x = 4$ case. *Middle:* The ratio of Maxwell to Reynolds stress, $\langle -b_x b_y / v_x v_y \rangle$ remains roughly constant for different L_z/L_x . *Bottom:* The ratio of the Maxwell stress to magnetic energy, $\alpha_{\text{mag}} = \langle -b_x b_y / b^2 \rangle$ is also rather insensitive to the aspect ratio for the cases considered here. The first and second results are in agreement with the work of Shi et al. (2016) while the lack of sensitivity of α_{mag} to aspect ratio is not.

3.2 Pm dependence

The dependence of α on dissipation coefficients is of interest since accretion disks come in a wide variety: protoplanetary disks that have $Pm \ll 1$ and active galactic nuclei with $Pm \sim 1$. Moreover, laboratory experiments of Taylor-Couette flow are typically done with liquid metal that have $Pm \in [10^{-7}, 10^{-5}]$. This makes detection of MRI in the lab a particularly challenging problem since MRI with a vertical field is hard to trigger for such low Pm . At low Pm , a net azimuthal or helical field might make it easier to trigger turbulence in magnetized Keplerian flows (Guseva et al. 2017b; see Rüdiger et al. 2018 for a review of laboratory MRI).

In Paper I, it was shown that turbulence could only sustain if $L_z/L_x \geq 4$ in the $Pm < 1$ regime with no imposed field. Previous studies addressing the dependence of transport coefficients on dissipation were confined to small aspect ratio shearing boxes and a net magnetic flux (Lesur & Longaretti 2007; Fromang et al. 2007; Meheut et al. 2015). These previous works found that the Pm dependence of α was very weak for $Pm < 1$, while it followed a power law for $Pm > 1$. Guseva et al. (2017b) found qualitative similar results for magnetized Taylor Couette flow. Our results are mixed (fig. 2): for $L_z/L_x = 4$ stress is insensitive to Pm at low Pm and has power law dependence $\alpha \sim Pm^{3/2}$ for higher Pm (bottom panel). However, $L_z/L_x = 8$ shows variations up to a factor of 3 for $Pm < 1$ (top panel). Note, however, that a single run at each $(L_z/L_x, Pm)$ is potentially misleading and ideally one would want several runs initiated with different initial conditions (each evolved for a long time ($\gg 100$ orbits)).

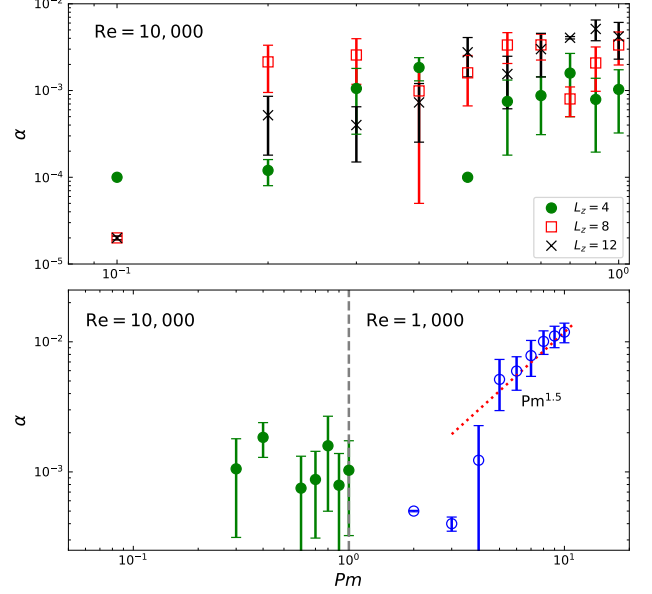


Figure 2. Volume averaged stress, $\alpha = \langle v_x v_y - b_x b_y \rangle / L_x^2 S^2$, on a log-log plot further averaged over time from $t = 250 - 1000 \text{ S}^{-1}$ (except for cases that decayed before that). *Top:* Stress for $Pm < 1$ at $Re = 10,000$ as a function of different aspect ratios L_z/L_x . The $L_z/L_x = 8$ (red squares) and $L_z/L_x = 12$ (black crosses) show variations up to an order of magnitude while $L_z/L_x = 4$ is more or less constant ($Pm = 0.1, 0.2, 0.5$ are nearly zero for this case). *Bottom:* At fixed $L_z = 4$, the stress seems to be insensitive to Pm for $Pm < 1$ (filled green circles) while it follows a $\alpha \sim Pm^{1.5}$ scaling for $Pm > 1$ (hollow blue circles). This is qualitatively consistent with previous work done with imposed fields (Meheut et al. 2015). In the bottom plot, data points for $Pm = 0.1, 0.2, 0.5$ are ignored.

3.3 Role of mean fields

We define the mean field \bar{Q} as:

$$\bar{Q} = \frac{1}{L_x L_y} \int Q dx dy. \quad (6)$$

This definition of mean field is not universal but it makes comparison with Shi et al. (2016) easier since they also employed a horizontal average. The disadvantage of using a horizontal average is that the vertical small scales (close to dissipation) are also considered part of the ‘mean’. In fig. 3, we plot the total and fluctuating α_{mag} , Maxwell stress and the magnetic energy. The fluctuations in magnetic field are defined through: $\mathbf{B} = \bar{\mathbf{B}} + \mathbf{b}'$ while $\alpha_{\text{mag}}^{\text{flu}}$ is defined as:

$$\alpha_{\text{mag}}^{\text{flu}} = \frac{-\overline{b'_x b'_y}}{b'^2} \quad (7)$$

where \mathbf{b}' is the fluctuating magnetic field. We do not observe clear differences in convergence between the two sets of quantities, α_{mag} and $\alpha_{\text{mag}}^{\text{flu}}$ (see top panel of fig. 3). This is in contrast to Shi et al. (2016) who found that it is the $\alpha_{\text{mag}}^{\text{flu}}$ that is invariant with vertical aspect ratio but the total α_{mag} decreases. Furthermore, Shi et al. (2016) observed that while the total stress α converged for aspect ratios $L_z/L_x > 2.5$, the total α_{mag} decreased as $(L_z/L_x)^{-1/2}$ with increasing aspect ratio. For the stresses, no clear difference in trends seems

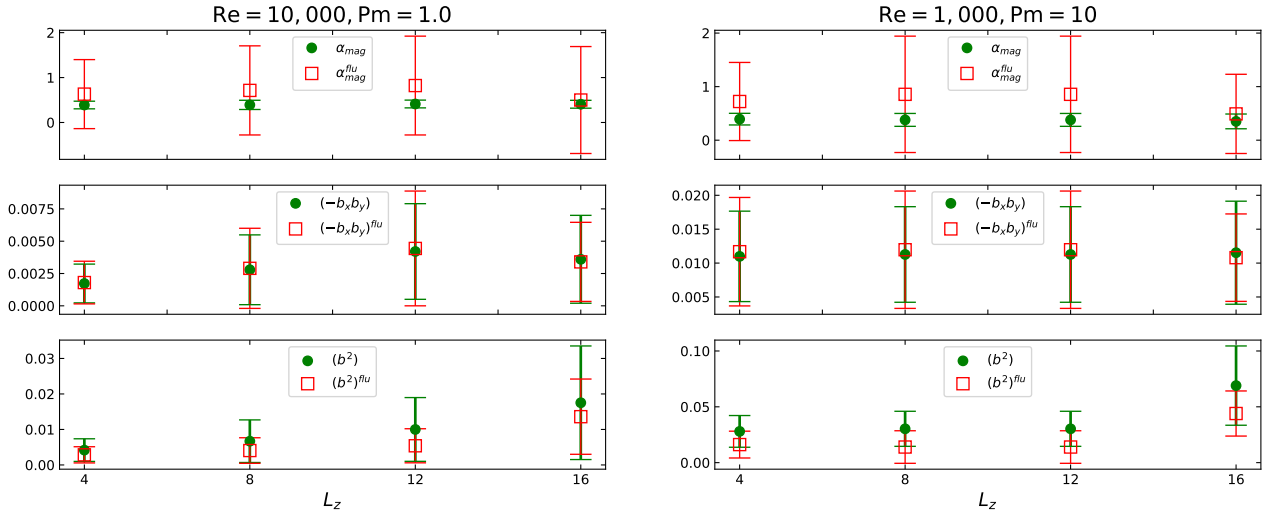


Figure 3. The horizontally (xy) averaged mean field and the corresponding fluctuating quantities that were further averaged over t, z for $L_z = 4, 8, 12, 16$ at $Re = 1,000, Pm = 10$ and $Re = 10,000, Pm = 1$. These quantities have been time averaged over $500 - 10000 S^{-1}$. *Top:* Neither α_{mag} nor the corresponding fluctuating quantity change much with either the vertical aspect ratio or the two different Pm . *Middle:* The total and fluctuating Maxwell stresses seem to be insensitive to box size but they are sensitive to Pm as we showed in the previous section. *Bottom:* The difference between the total and fluctuating magnetic energy is within a factor of 2. For both $Pm = 1$ (left) and $Pm = 10$ (right), the total and fluctuating magnetic energy grow with aspect ratio.

to exist as a function of aspect ratios between the total or the fluctuating quantities (see also fig. 1). The mean $\alpha_{mag}^{mean} = -\overline{B_x B_y} / \overline{B^2} \sim 10^{-2}$ for all the aspect ratios considered here and is considerably smaller than the fluctuating contribution in agreement with Blackman & Nauman (2015); Shi et al. (2016). However, the total and fluctuating magnetic energies (bottom panel on left and right) seem to increase with aspect ratio.

4 RESOLUTION TESTS

The results reported in this paper describe the statistics of quadratic quantities (stresses and energies) as a function of dissipation coefficients and aspect ratios. One might ask if these results are sensitive to the numerical resolution employed ($64/L_x$). We first note that pseudo-spectral methods (as employed in SNOOPY) are more accurate than finite difference methods: a rule of thumb is that second order (central difference) finite difference schemes require twice as much resolution as a pseudo-spectral scheme to achieve the same level of accuracy (Moin & Mahesh (1998)). Secondly, higher order moments (for example, fourth order structure functions) require higher resolution to be properly resolved but the resolution requirements are not as stringent on quadratic quantities like energies or stresses (Yakhot & Sreenivasan (2005); Donzis et al. (2008)).

Nonetheless, it is useful to do a resolution study to check if there are any drastic differences between the resolutions employed in this paper and higher resolutions. For this purpose, for two runs with $L_x = 1, L_y = 2, L_z = 4, Rm = 10000$ having different Pm ($= 1, 10$), we study (i) the time history of volume averaged stresses in fig. 4; and (ii) the power spectrum of $\langle v_x \rangle$ as a function of k_z in fig. 5. The plots in fig. 5 were calculated in postprocessing and were consequently time averaged over significantly smaller duration as well as

snapshots as the size of each snapshot significantly increases with resolution. We do not notice any noticeable difference between the lower resolution $64/L_x$ and higher resolutions $128/L_x, 256/L_x$ (fig. 5).

Higher resolution runs are computationally very expensive. For instance, the run at $256/L_x$ for $L_z = 4, Re = Rm = 10000$ costed $\sim 1.5 \times 10^5$ CPU hours for just $2000 S^{-1}$ while all the runs combined in fig. 1 took less than 10^5 CPU hours. These runs become even more expensive as the energies increase with Pm . The $L_z = 4, Re = 1000, Pm = 10$ run took 10^5 CPU hours for just $500 S^{-1}$, which means that it would take 2×10^6 CPU hours to evolve this run to $10000 S^{-1}$.

5 EXTENDED Y AND Z DOMAINS

In the previous section, we discussed transport properties of simulations with $L_x = 1, L_y = 2$ and variable L_z . This is largely the set of runs Paper I was based on. In order to explore the sensitivity of the domain size in the ‘y’ direction, we conducted two more numerical simulations with $L_y = L_z = 4, 8$. Large domains in both ‘y’ and ‘z’ directions are computationally prohibitive since, for example, a resolution of $64/L_x$ with $L_y = L_z = 16$ would amount to simulating a box with $64 \times 1024 \times 1024$ grid points. We use the same resolution as before ($64/L_x$) but a lower Reynolds numbers, $Re = Rm = 4000$. In fig. 5, we plot the evolution of turbulent stresses for the two runs considered in this section. We find that the stress for the $L_y = L_z = 4$ remains relatively similar to $L_y = 2, L_z = 4$ case in fig. 1 ($\alpha \sim 5 \times 10^{-3}$ here as opposed to 2×10^{-3}) but $L_y = L_z = 8$ reaches higher saturated values ($\alpha \sim 2 \times 10^{-1}$ that is about 50 times larger than the $L_y = 2, L_z = 8$ case in fig. 1). This result is very intriguing since the Re, Rm used for these runs is actually lower than the ‘tall’ box runs so one would naively expect a lower α here.

When averaged over the time period $250 - 500 S^{-1}$, the

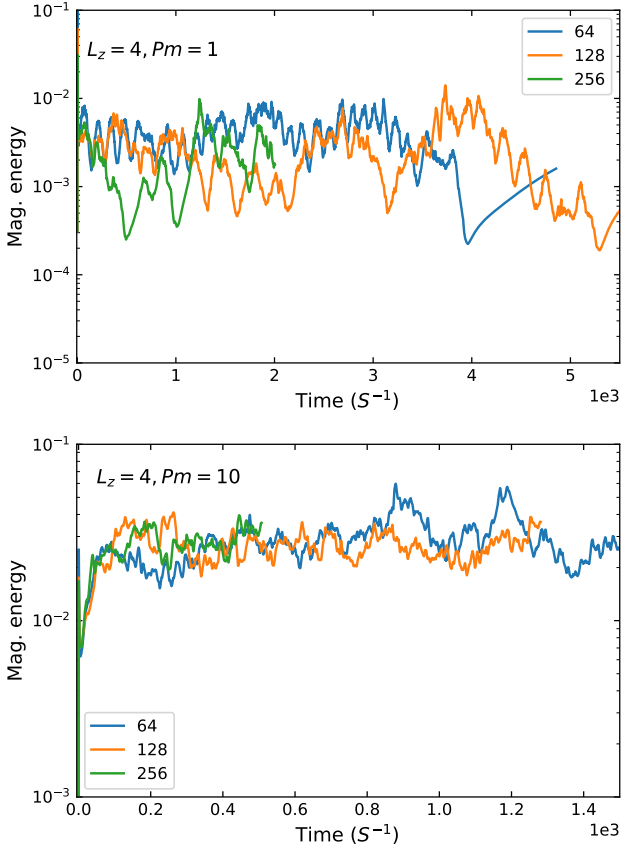


Figure 4. Time history plotted for different resolutions at $L_z = 4$, $Pm = 1$ (top) $Pm = 10$ (bottom). *Top:* The decay time scale as well as behavior at the early stages is sensitive to resolution. The time averaged amplitude of the stresses in the saturated state averaged over $500 - 2000 S^{-1}$ is 0.002, 0.0008, 0.0009 for resolutions $64/L_x$, $128/L_x$, $256/L_x$. *Bottom:* No strong variations among the three runs seem to exist ($\alpha \sim 0.012$ for all three runs).

extended $L_y = L_z = 8$ behaves similar to the $L_y = 2, L_z = 8$ simulation reported in the previous section: $\langle -b_x b_y \rangle \sim \langle -b'_x b'_y \rangle$ and $\langle b^2 \rangle \sim \langle b'^2 \rangle$. However, in the saturated state ($\geq 500 S^{-1}$), there is a significant change in behavior: the magnetic energy is dominated by the mean fields: $\langle b^2 \rangle \sim \langle \bar{B}^2 \rangle$ but the stress is still dominated by the fluctuating component. In fig. 5, we show the snapshot of the azimuthal magnetic for the two $L_z = 8$ runs: one with $L_y = 2, Re = Rm = 10000$ and the other with $L_y = 8, Re = Rm = 4000$. In both cases, the field has considerable structure in the vertical direction. A strong banded structure parallel to the y axis forms in the extended yz domain case while the ‘tall’ box case has weaker bands but more of them (see also Walker & Boldyrev (2017)).

6 CONCLUSIONS

Most studies of magnetized Keplerian flows have focused on an imposed magnetic flux in a small domain. Some of the literature has focused on studying the effects of dissipation coefficients on sustained turbulence (Lesur & Longaretti 2007; Meheut et al. 2015). Recent work has suggested that

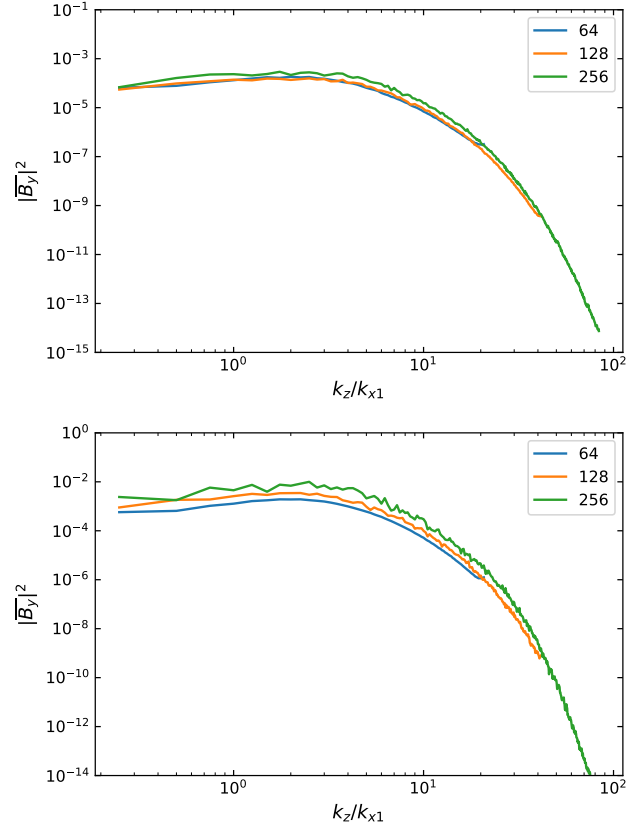


Figure 5. Power spectrum for the horizontally averaged \bar{B}_y as a function of vertical wavenumber for different resolutions at $L_z = 4$, $Pm = 1$ (top) $Pm = 10$ (bottom). The spectrum is normalized such that $\int |\bar{B}_y|^2 dk_z = \langle B_y^2 \rangle$. The vertical wavenumber on the horizontal axis is normalized to $k_{x1} = 2\pi/L_x$. The overall shape of the spectra is very similar for all the 3 resolutions for both the top and bottom set of runs. We note that the temporal average is over fewer snapshots for higher resolution runs since we only stored snapshots every $10 S^{-1}$ (for $256 \times 256 \times 1024$) as opposed to $1 S^{-1}$ for $64/L_x$, $128/L_x$.

domain size might play a key role when there is no imposed flux (Shi et al. 2016; Nauman & Pessah 2016). This work is a survey of the effects of large aspect ratios and dissipation coefficients on transport coefficients. We have found that:

- (i) For fixed $L_y/L_x = 2$, α is not sensitive to Pm for $Pm < 1$ and follows a power law $\alpha \sim Pm^{1.5}$ for $Pm > 1$.
- (ii) For fixed $L_y/L_x = 2$, the turbulent stresses α , α_{mag} and $\langle -b_x b_y \rangle / \langle v_x v_y \rangle$ are all nearly insensitive to increase in L_z/L_x .
- (iii) For $L_y = L_z \gg L_x$, the saturated level of α increases significantly especially with $L_y = L_z = 8$ where $\alpha \sim 0.2$.

Our study highlights the importance of aspect ratio that we first pointed out in Paper I and motivates further work that might give important insights into the role of turbulence in magnetized Keplerian flows.

ACKNOWLEDGMENTS

The research leading to these results has received funding from the European Research Council under the Euro-

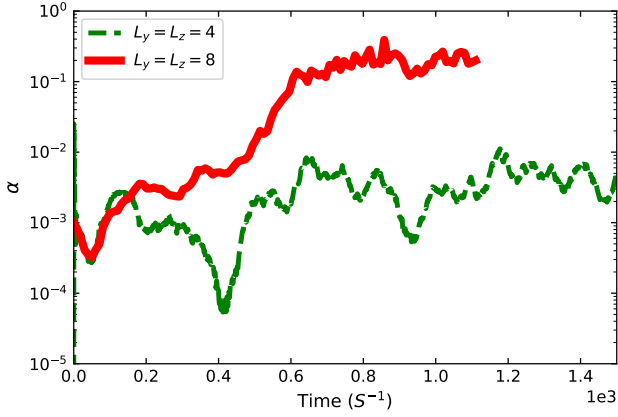


Figure 6. Volume averaged stress, $\alpha = \langle v_x v_y - b_x b_y \rangle / L_x^2 S^2$ as a function of time for $L_y = L_z = 4, 8$ at $Re = 4,000, Pm = 1$. We find that the stresses increase with L_y/L_x quite significantly and that the saturated level of stresses for $L_y/L_x = 8$ is ~ 40 times larger than the case with $L_y = L_z = 4$.

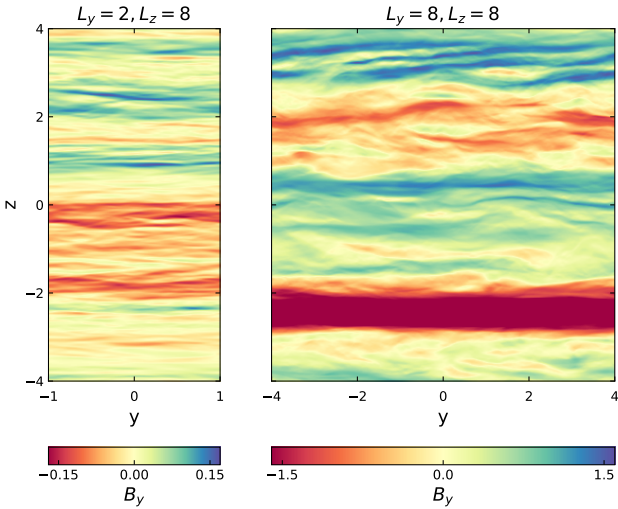


Figure 7. Snapshot of B_y at $t = 1000 S^{-1}$ averaged over ‘x’. The colorbar at the bottom indicates nearly an order of magnitude difference in magnitudes of B_y for the two cases. *Left:* Some hint for large scale structure exists. *Right:* The extended ‘yz’ domain case presents some strong bands that seem to be also responsible for $\overline{b^2} \sim \overline{B^2}$.

pean Union’s Seventh Framework Programme (FP/2007-2013) under ERC grant agreement 306614.

REFERENCES

- Balbus S. A., Hawley J. F., 1991, *ApJ*, **376**, 214
 Balbus S. A., Hawley J. F., 1998, *Reviews of Modern Physics*, **70**, 1
 Blackman E. G., Nauman F., 2015, *Journal of Plasma Physics*, **81**, 395810505
 Bodo G., Cattaneo F., Mignone A., Rossi P., 2014, *ApJ*, **787**, L13
 Brandenburg A., Nordlund A., Stein R. F., Torkelson U., 1995, *ApJ*, **446**, 741

- Chandrasekhar S., 1960, *Proceedings of the National Academy of Science*, **46**, 253
 Cross M. C., Hohenberg P. C., 1993, *Rev. Mod. Phys.*, **65**, 851
 Davis S. W., Stone J. M., Pessah M. E., 2010, *ApJ*, **713**, 52
 Donzis D. A., Yeung P. K., Sreenivasan K. R., 2008, *Physics of Fluids*, **20**, 045108
 Flock M., Dzyurkevich N., Klahr H., Turner N., Henning T., 2012, *ApJ*, **744**, 144
 Fromang S., Lesur G., 2017, preprint, ([arXiv:1705.03319](https://arxiv.org/abs/1705.03319))
 Fromang S., Papaloizou J., 2007, *A&A*, **476**, 1113
 Fromang S., Papaloizou J., Lesur G., Heinemann T., 2007, *A&A*, **476**, 1123
 Gressel O., Pessah M. E., 2015, *ApJ*, **810**, 59
 Guseva A., Hollerbach R., Willis A. P., Avila M., 2017a, *Physical Review Letters*, **119**, 164501
 Guseva A., Willis A. P., Hollerbach R., Avila M., 2017b, *ApJ*, **849**, 92
 Hawley J. F., Gammie C. F., Balbus S. A., 1995, *ApJ*, **440**, 742
 Hawley J. F., Gammie C. F., Balbus S. A., 1996, *ApJ*, **464**, 690
 Hawley J. F., Guan X., Krolik J. H., 2011, *ApJ*, **738**, 84
 Lemoult G., Shi L., Avila K., Jalikop S. V., Avila M., Hof B., 2016, *Nature Physics*, **12**, 254
 Lesur G., Longaretti P.-Y., 2007, *MNRAS*, **378**, 1471
 Lesur G., Ogilvie G. I., 2008, *A&A*, **488**, 451
 Meheut H., Fromang S., Lesur G., Joos M., Longaretti P.-Y., 2015, *A&A*, **579**, A117
 Moin P., Mahesh K., 1998, *Annual Review of Fluid Mechanics*, **30**, 539
 Nauman F., Pessah M. E., 2016, *ApJ*, **833**, 187
 Parkin E. R., Bicknell G. V., 2013, *MNRAS*, **435**, 2281
 Pessah M. E., Chan C.-k., Psaltis D., 2007, *ApJ*, **668**, L51
 Philip J., Manneville P., 2011, *Phys. Rev. E*, **83**, 036308
 Pomeau Y., 1986, *Physica D: Nonlinear Phenomena*, **23**, 3
 Rüdiger G., Gellert M., Hollerbach R., Schultz M., Stefani F., 2018, *Phys. Rep.*, **741**, 1
 Ryan B. R., Gammie C. F., Fromang S., Kestener P., 2017, *ApJ*, **840**, 6
 Shi J.-M., Stone J. M., Huang C. X., 2016, *MNRAS*, **456**, 2273
 Suzuki T. K., Inutsuka S.-i., 2014, *ApJ*, **784**, 121
 Velikhov E. P., 1959, *JETP*, **36**, 995
 Walker J., Boldyrev S., 2017, *MNRAS*, **470**, 2653
 Wei X., Ji H., Goodman J., Ebrahimi F., Gilson E., Jenko F., Lackner K., 2016, *Phys. Rev. E*, **94**, 063107
 Yakhot V., Sreenivasan K. R., 2005, *Journal of Statistical Physics*, **121**, 823
 Zhu Z., Stone J. M., 2018, *ApJ*, **857**, 34